Structure, Vol. 13, 309–317, February, 2005, ©2005 Elsevier Ltd All rights reserved. DOI 10.1016/j.str.2004.12.013

An Inflammatory Role for the Mammalian Carboxypeptidase Inhibitor Latexin: Relationship to Cystatins and the Tumor Suppressor TIG1

Anna Aagaard,[1] Pawel Listwan,[2,3] Nathan Cowieson,[1] Thomas Huber,[4] Timothy Ravasi,[1,3,5] Christine A. Wells,[1] Jack U. Flanagan,[3] Stuart Kellie,[1,2,3] David A. Hume,[1,3,5] Bostjan Kobe,[1,2,5] and Jennifer L. Martin[1,2,5,*]

[1]Institute for Molecular Bioscience
[2]School of Molecular and Microbial Sciences
[3]Cooperative Research Centre for Chronic Inflammatory Diseases
[4]Department of Mathematics
[5]ARC Special Research Centre for Functional and Applied Genomics
University of Queensland
Brisbane, QLD 4072
Australia

Summary

Latexin, the only known mammalian carboxypeptidase inhibitor, has no detectable sequence similarity with plant and parasite inhibitors, but it is related to a human putative tumor suppressor protein, TIG1. Latexin is expressed in the developing brain, and we find that it plays a role in inflammation, as it is expressed at high levels and is inducible in macrophages in concert with other protease inhibitors and potential protease targets. The crystal structure of mouse latexin, solved at 1.83 Å resolution, shows no structural relationship with other carboxypeptidase inhibitors. Furthermore, despite a lack of detectable sequence duplication, the structure incorporates two topologically analogous domains related by pseudo two-fold symmetry. Surprisingly, these domains share a *cystatin* fold architecture found in proteins that inhibit *cysteine proteases*, suggesting an evolutionary and possibly functional relationship. The structure of the tumor suppressor protein TIG1 was modeled, revealing its putative membrane binding surface.

Introduction

Latexin, or tissue carboxypeptidase inhibitor (TCI), is the only known mammalian carboxypeptidase inhibitor (CPI), and recombinant rat latexin has been shown to inhibit pancreatic carboxypeptidase A1 (CPA1), CPA2 (K_i ~3 nM), and CPA3 (mast cell carboxypeptidase, K_i 16 nM) (Normant et al., 1995). Comprising over 220 residues, the protein is significantly larger than CPIs from plants and parasites (40–70 residues). Furthermore, latexin lacks the conserved 7-residue C terminus of these shorter CPIs that interacts with CPA in a substrate-like manner (Reverter et al., 2000). The loss of the C terminus suggests that latexin and the plant/parasite CPIs have distinctly different mechanisms of CPA inhibition.

Latexin was first identified as a marker of neurons in the *lat*eral neocor*tex* (hence *latexin*) of the developing mammalian brain (Arimatsu, 1994). It has been used to elucidate the mechanism of cortical regional specification, and it was suggested to play a role in the modulation of sensory perception (Bai et al., 2004). It is thought that latexin functions in inflammation and innate immune pathways because it is expressed by rat mast cells, it inhibits mast cell CPA3, and it localizes to a novel population of mast cell granules, distinct from the classical exocytic granule classes (Uratani et al., 2000). Furthermore, latexin is induced in acute pancreatitis and lung inflammatory disease (Ji et al., 2003). Here, we present new evidence for a role for latexin in inflammation by showing that its expression is induced in stimulated mouse macrophages in concert with potential protease targets and other protease inhibitors.

Although unrelated to known CPIs, latexin does share sequence similarity with TIG1 (Figure 1, ~30% identity over 220 residues), a protein found in mouse, rat, and human. TIG1 is expressed in skin fibroblasts and epithelia, and it is encoded by a retinoic acid (RA) receptor-responsive gene. It has been implicated in both the therapeutic effects of RA in psoriasis (Nagpal et al., 1996) and, more recently, in tumor suppression (Jing et al., 2002). TIG1 is larger than latexin, and the additional residues are thought to encode a membrane anchor at the N terminus (Nagpal et al., 1996).

Other proteins with sequence identity (~30%) to latexin are found in chicken (ovocalyxin [Hincke et al., 2003]) and *Xenopus* (Figure 1), but no related proteins were found in nonvertebrates. Chicken ovocalyxin is a protein involved in egg shell production. This similarity, the vertebrate-restricted gene family, and the reported expression of latexin in osteoblasts (Balint et al., 2003) suggest roles for latexin in bone regulation and calcification.

To gain insight into the function of latexin, we investigated its expression profile in macrophages, determined its crystal structure, and used the structure to model that of TIG1. The latexin structure reveals unexpected pseudosymmetry and a previously unknown relationship with the cysteine protease inhibitor cystatin.

Results

Latexin Is Macrophage Enriched and Inducible

In light of a possible role for latexin in inflammation, we examined expression in macrophages, the major cell type recruited to acute and chronic inflammatory sites. We have previously reported extensive analyses of gene expression profiles in mouse macrophages from several mouse strains (Wells et al., 2003a). These analyses indicate that the gene encoding latexin forms part of a set that is highly enriched in macrophages compared to other cell types and tissues, and is highly expressed in macrophage-rich tissues such as spleen and liver (Wells et al., 2003b). The latexin gene also fell within a cluster of genes induced in macrophages by the major lineage-specific growth factor, colony stimu-

*Correspondence: j.martin@imb.uq.edu.au

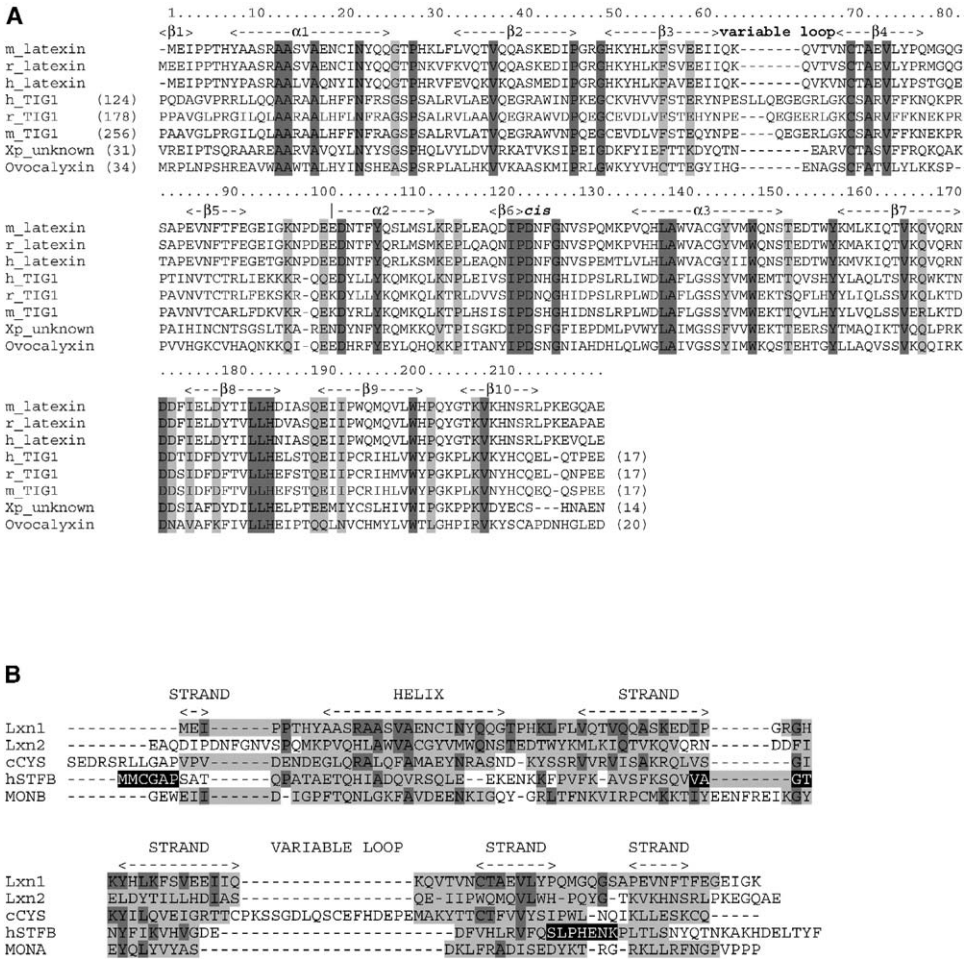

Figure 1. Sequence Alignments

(A) Multiple sequence alignment of mouse, rat, and human latexin (m_latexin, NP_058033.2; r_latexin, NP_113843.1; h_latexin, AAF82807.1); human, rat, and mouse TIG1 (h_TIG1, AAH29640.1; r_TIG1, XP_227232.2; m_TIG1, XP_130987.2); *Xenopus laevis* latexin-like protein (Xp_unknown, AAH59975.1); and chicken ovocalyxin (CAC44378.2). The number of N- or C-terminal residues not shown in the alignment are indicated in parentheses. Residue numbers and secondary structure for mouse latexin are shown. Residues conserved throughout are shaded in dark gray, and where the residue is conserved in all but one, it is shaded in light gray.

(B) Structure-based sequence alignment of the N- and C-terminal latexin domains (Lxn1 and Lxn2, respectively), chicken cystatin (cCYS, PDB accession code 1CEW [Bode et al., 1988]), human Stefin B (hSTFB, 1STF [Stubbs et al., 1990]), and monellin (MONB and MONA, respectively, for the two peptides, 1MOL [Somoza et al., 1993]). Residues that can be structurally aligned with the N-terminal domain of latexin are highlighted in light gray. Residues that are identical—after structural alignment—with the N-terminal domain of latexin are highlighted in dark gray, and residues from human Stefin B that interact with the cysteine protease papain (1STF [Stubbs et al., 1990]) are shaded in black.

lating factor 1 (CSF-1), in combination with the pathogen product, lipopolysaccharide (LPS).

To confirm the latexin expression profile identified by using cDNA microarrays, we performed real-time PCR analysis in LPS-stimulated bone marrow-derived macrophages in the presence or absence of CSF-1. Latexin mRNA was, indeed, expressed at high levels in macrophages, and it was further induced by a combination of LPS and CSF-1 (Figure 2). Other genes induced by LPS in murine macrophages included CPA3 (mast cell CP), a known interaction partner of latexin, carboxypeptidase D (this has been noted previously, Hadkar and Skidgel, 2001), and the cysteine protease inhibitors cystatin C and cystatin F (Figure 2). Indeed, ~8% of genes upregulated under this stimulation encode proteases or protease inhibitors. By comparison, TIG1 gene expression is also high in macrophages but does not change upon stimulation.

Structure of Latexin

Based upon its expression profile in macrophages, latexin and its target CPA represent potential targets for therapeutic intervention in chronic inflammatory disease. As no latexin homologs with known structures could be identified, we determined its structure by X-ray crystallography by using MAD methods and SeMet-labeled protein. The structure has one molecule in the asymmetric unit and was refined at 1.83 Å resolution (Table 1).

Although there is no evidence of internal symmetry from the polypeptide sequence, the crystal structure re-

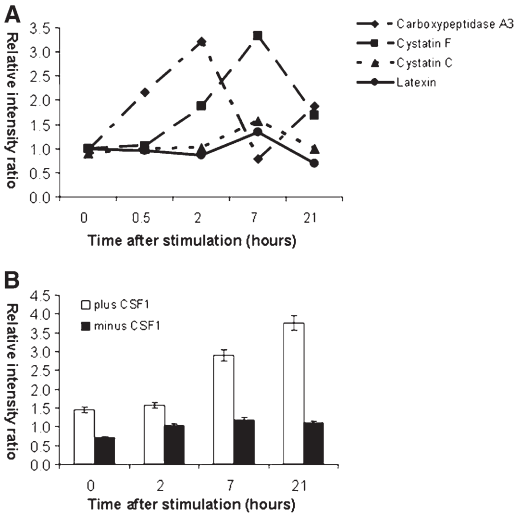

Figure 2. Expression in Macrophages

(A) Quantitative real-time PCR profiles of latexin mRNA showing dynamic expression after LPS stimulation in macrophages over time, in concert with other protease inhibitors and potential target proteases. The expression peak for latexin is at 7 hr, when the macrophage response to LPS also reaches a maximum.

(B) Quantitative real-time PCR profiles of latexin mRNA showing the effect of the growth factor CSF-1. The plotted data have been normalized as described in the Experimental Procedures.

veals two structurally related domains (domains 1 and 2) linked by a connecting helix (α2) (Figure 3). Each domain comprises a five-stranded antiparallel β sheet wrapped around an α helix. The sequence identity between the two domains is ~11% after structural alignment (Figure 1B), yet the C_α atoms of 84 residues of domains 1 and 2 overlay with an rmsd of 1.9 Å. Extraordinarily, the pseudosymmetry is such that both domains can be superimposed on the other, simultaneously giving an rmsd of 2.1 Å for the C_α atoms of 142 aligned residues (Figure 3).

The major structural differences between the two domains are variations in β strand lengths and different loop conformations and sizes. This is particularly striking for the loop connecting the first β strand and the α helix of each domain (β1-α1 and β6-α3, respectively). In domain 2, this loop comprises 11 residues (residues 121–131) that protrude from the core, while the equivalent loop in domain 1 is formed from five residues (residues 4–8) (Figure 1B).

Latexin Comprises Two Cystatin-like Folds

No other protein was found to have the same overall topology as latexin (DALI [Holm and Sander, 1993]); however, the individual domains share the topology of the cystatin/monellin family of proteins (Figure 4) (Murzin et al., 1995). Cystatins are cysteine protease inhibitors, and monellin is a sweet-tasting protein from the West African berry *Dioscoreophyllum cumminsii* (Somoza et al., 1993). The cystatin/monellin fold is characterized by a five-stranded antiparallel β sheet and a central α helix. The structure of chicken cystatin (Bode et al., 1988) is the most similar to latexin (rmsd of 1.6 Å and 14 [17%] identical residues for the comparison of 84 C_α atoms with the latexin N-terminal domain).

Although there is no overall sequence relationship between latexin and cystatins (Figure 1B), the structural relationship suggests an evolutionary and possibly a functional relationship. When submitted as individual domains, the meta-server 3D-JURY (Ginalski et al., 2003) predicted the sequence of domain 1, but not domain 2, to have a cystatin-like structure. Furthermore, in the genes encoding both human and mouse latexin, the position between domains 1 and 2 corresponds to an intron-exon boundary, with each domain encoded by three exons (data not shown). These data suggest that latexin may have evolved from an ancestral cystatin-like protein as a consequence of a gene duplica-

Table 1. Data Collection and Refinement Statistics

Data Collection				
	MAD (SeMet)			Native
Wavelength (Å)	0.9794	0.9796	0.9077	1.0781
Resolution range (Å)	50–1.96	50–1.96	50–1.96	50–1.83 (1.9–1.83)[a]
Observed reflections	413,797	392,101	399,913	426,598
Unique reflections	22,703	22,622	22,591	29,633
R_{merge}[b]	0.073	0.071	0.060	0.039 (0.422)[a]
Completeness (%)	99.9	99.9	99.1	99.7 (100)[a]
<I>/<σ(I)>	18.5	15.3	12.8	19.9 (4.5)[a]

Refinement	
Resolution of data used in refinement	50.0–1.83 (1.94–1.83)[a]
Number of reflections total/test set	28,971/2,897
R_{fac}[c] and R_{free}[d] (%)	21.1 (25.9)[a] and 23.7 (26.8)[a]
Number of protein atoms/waters	1,871/184
Rmsd from ideal geometry: bonds (Å)/angles (°)	0.011/1.5
Ramachandran: most favored/disallowed regions (%)	91.3/0.0

[a] Parentheses refer to the highest resolution shell.

[b] $R_{merge} = \Sigma|I - <I>|/\Sigma<I>$; I is the intensity of each reflection.

[c] $R_{fac} = \Sigma_h|F_o - F_c|/\Sigma_h|F_o|$; F_o and F_c are observed and calculated structure-factor amplitudes for each reflection, h.

[d] R_{free} for 10% of data selected randomly and excluded from refinement.

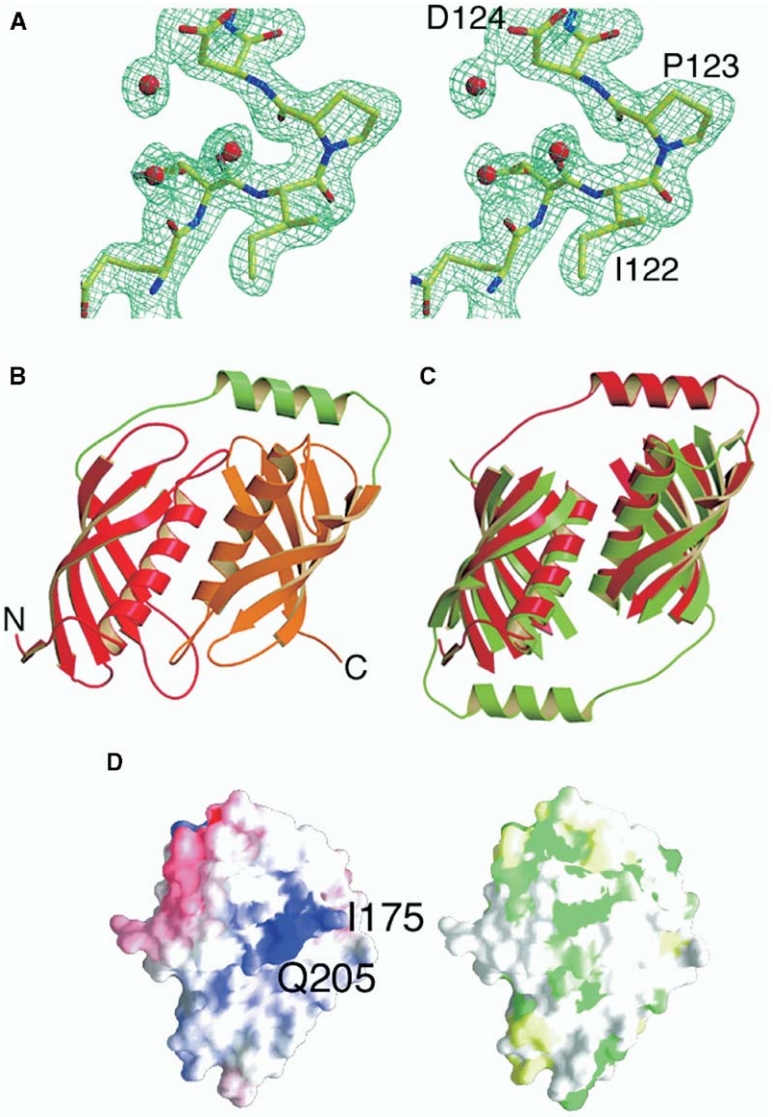

Figure 3. Crystal Structure

(A) Stereo diagram of the electron density ($2F_o$-F_c contoured at 2σ) around the *cis*-proline region (Ile122-*cis*Pro123-Asp-124).

(B) Schematic of the latexin structure showing β strands as arrrows and α helices as spirals. The N-terminal subdomain (residues 1–97) is red, the C-terminal subdomain (residues 118–222) is orange, and the linking α helix is green.

(C) Superposition of the two subdomains, residues 1–97 (red) on residues 118–222 (green) and residues 118–222 (red) on residues 1–97 (green). Some loops were removed for clarity.

(D) Surface renderings of latexin showing (left) a putative binding surface predicted from PROMATE (Neuvirth et al., 2004); the best-predicted binding surface is shown in blue, the less probable binding surface is shown in white, and the least probable binding surface is shown in red. The surface on the right shows the conservation of residues across the three mammalian latexins, ovocalyxin, and *Xenopus* latexin-like protein (which together make one branch in the phylogenetic tree, with the TIG1 proteins forming another branch). The color scheme is green for highly conserved residues, white for less conserved proteins, and yellow for least conserved proteins.

The figure was generated by using GRASP (Nicholls et al., 1993), MOLSCRIPT (Kraulis, 1991), and Raster3D (Merritt and Murphy, 1994) or by using BOBSCRIPT (Esnouf, 1999) and Povray (www.povray.org).

tion event. The overall gene structure for cystatins is similar to that for the individual domains of latexin in that there are three exons and two introns. However, the length and sequence of the introns and exons are not conserved between cystatins and latexin domains, suggesting that if the latexin N-terminal domain evolved from an ancestral cystatin, the divergence would have occurred early in evolution. The presence of two cystatin-like domains also suggests the possibility that cleavage may be required for activity. However, there is no evidence of cleavage of recombinant mouse latexin; it forms a stable complex with bovine CPA (data not shown).

Carboxypeptidase Binding

Crystal structures of the potato and leech CPIs in complex with CPA2 revealed that the C-terminal tail of the inhibitors interacts with the active site of CPA in a substrate-like manner (Rees and Lipscomb, 1982; Reverter et al., 2000). The C-terminal residues (-Pro-Tyr-Val-X) are conserved in these inhibitors, but not in latexin; therefore, a common mechanism of inhibition can be ruled out (Normant et al., 1995). Previous sequence analysis studies identified a limited degree of similarity between an 11-residue sequence of latexin (200-LWHPQ YGTKVK-210) and the prosegment of carboxypeptidase B (CPB) (37-FWKPDSATQVK-47) (Normant et al., 1995). It was therefore suggested that this region of latexin may inhibit CPs by mimicking the prosegment of the enzymes. However, the two sequence motifs form very different secondary structures in their respective proteins, indicating that this mechanism of inhibition is unlikely.

We used structural approaches to identify potential binding sites on latexin. The program ProMate (Neuvirth et al., 2004) identified a surface patch that includes residues 174-FI-175, 204-PQ-205, and T208 (Figure 3D). This region from the C-terminal domain of latexin includes the residues that are similar in sequence to the proCPB region described above, and it

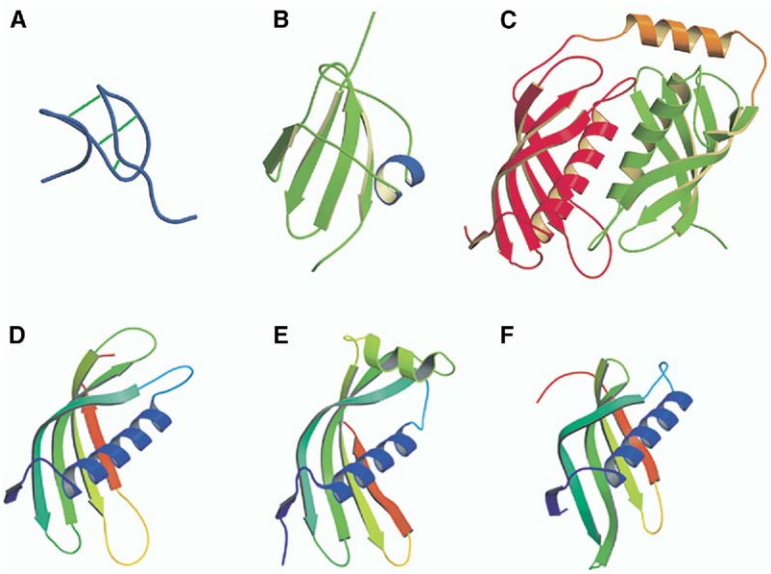

Figure 4. Diversity and Similarity in CP Inhibitors, Cystatin, and Monellin

(A–F) Structures of CP inhibitors from (A) potato (4CPA [Rees and Lipscomb, 1982]) and (B) leech (1DTV [Reverter et al., 2000]) are very different from the structure of mammalian CP inhibitor, (C) latexin. However, latexin (N-terminal domain, [D]) is structurally related to proteins in the (E) cystatin (cysteine protease inhibitor, chicken cystatin) (1CEW [Bode et al., 1988]) and (F) monellin (sweet-tasting protein) (1MOL [Somoza et al., 1993]) fold family.

also includes a loop equivalent to one of the papain-interacting regions of the cystatin human Stefin B (170-RNDDFI-175 of latexin, corresponding to VAGT of human Stefin B, highlighted in Figure 1B). Some conserved residues also map to this area of the surface (Figure 3D), though this analysis is hampered by the low number of latexin sequences available.

Heparin and Sulfate Binding

Latexin also interacts directly with a heparin component in the mast cell population of granules (Uratani et al., 2000). We identified the potential binding surface by using GRID (Goodford, 1985) with a sulfate anion probe. At high-energy contour levels (–9.0 kcal/mol), a sulfate binding site was observed near Arg171. Analysis of the electrostatic properties of the protein surface (GRASP [Nicholls et al., 1993]) supports the identification of this basic patch as a sulfate binding site. Moreover, the close proximity of another basic patch, formed by residues Lys208, Lys210, and His211 on strand 9, could coordinate other sulphates on a heparin sulfate oligomer. This hypothesis is supported by docking a mast cell granule heparin sulfate pentasaccharide onto the mouse latexin surface. Of 50 solutions, 43 had a sulfate group in the vicinity of the proposed sulfate binding pocket identified by GRID, and 26 had another sulfate positioned close to the basic patch.

Conservation of a cis-Proline Motif

The structure of latexin incorporates a *cis*-peptide bond between residues Ile122 and Pro123. These residues are located in a protruding loop between the first β strand (β6) and α helix (α3) of domain 2. The density in this region is well defined (Figure 3), and the sequence in this region (IPDXXG) is conserved throughout the latexin/TIG1 family of proteins (Figure 1). Indeed, with four of six residues conserved in all eight proteins, this is the most highly conserved motif in the entire sequence. This high degree of conservation in a family of proteins that are related overall by only 30% identity suggests that the *cis* form of the peptide bond will also be present in TIG1 and the *Xenopus* and ovocalyxin proteins. Furthermore, the position of the *cis*-proline motif on a protruding loop is suggestive of a protein interaction surface.

Structure of TIG1

Alignment of latexin and TIG1 sequences illustrates that differences exist between the two proteins as well as within the TIG1 family. The most notable of these is the presence of a variable length N-terminal extension in TIG1 relative to latexin (Figure 1) that is predicted to form a transmembrane helix.

Models of human latexin and human TIG1 were derived by homology modeling based on the crystal structure of mouse latexin. The electrostatic surfaces of human latexin and human TIG1 (Figure 5) show that the two proteins have strikingly different charge distributions on one face, with TIG1 having a predominantly basic surface. This surface may interact with membranes, given that human TIG1 is predicted to be membrane bound. The opposite face of TIG1 has features common to latexin. A basic patch is present in a similar location to that created by Lys18 and Lys159 in mouse latexin and Lys159 in human latexin. The surface around this patch is more hydrophobic in human TIG1 compared to human latexin (due to substitutions of Lys159 to Tyr, Ile62 to Tyr, Glu33 to Val, and Gln18 to Leu), and the negative patch at the helix 2 end of the cleft is reduced in size. Furthermore, the residues defining the heparin binding site identified in the mouse latexin structure, and also present in the human and rat latexin isoforms, are not conserved in TIG1.

Discussion

Latexin is the only known mammalian carboxypeptidase inhibitor. We have found that latexin is expressed

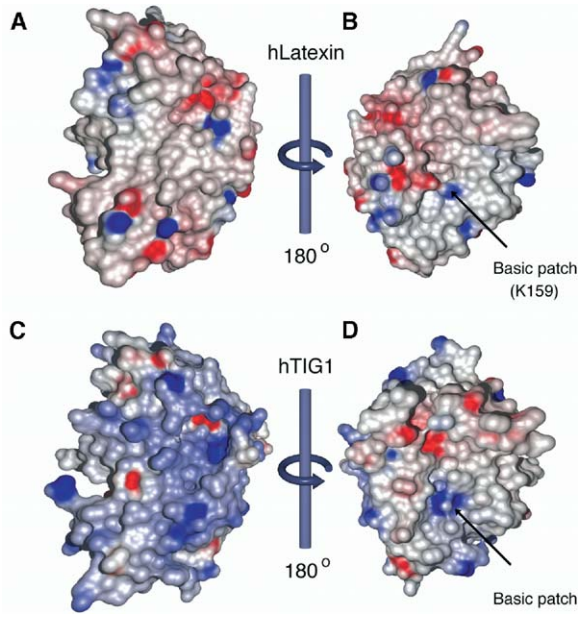

Figure 5. Comparison of Human Latexin and Human TIG1

(A–D) Electrostatic surfaces are shown for (A and B) human latexin and (C and D) TIG1 based on models derived from the crystal structure of mouse latexin. The broadly basic surface of (C) TIG1—absent in (A) latexin—suggests an interaction surface for phospholipid membranes, consistent with a predicted membrane anchor at the N terminus of TIG1. (B and D) A basic patch on the opposite face of both proteins is indicated. This is also present, and more prominent, in mouse latexin (not shown). The figure was produced by using GRASP (Nicholls et al., 1993).

constitutively at high basal levels in mouse macrophages and can be further upregulated by stimulation of the cells with a growth factor or proinflammatory stimulus. Upregulation occurs in parallel with several other types of protease inhibitors and target proteases. The known targets of latexin are the three isoforms of CPA, though it is possible that latexin may interact with and regulate the activity of other proteases.

Nevertheless, the available data strongly suggest a role for CPA and latexin in inflammation, and other CPs, including CPM, have been shown to correlate with macrophage cytotoxic activity (Rehli et al., 2000). CPA has been reported to be involved in the production or regulation of several proinflammatory mediators. In vitro, CPA from mast cells degrades endothelin-1, raising the possibility that it limits endothelin-mediated vasoconstriction and proliferation (Metsarinne et al., 2002). Pancreatic CPA has also been shown to convert the potent leukotriene C4 to the less potent leukotriene F4 by hydrolysis of an amide bond, again suggesting a negative role in inflammation (Reddanna et al., 2003). However, purified bovine CPA can induce NFκB-dependent TNFα production from macrophages, suggesting a proinflammatory role (Jaffray et al., 2000). The balance between CPA and latexin could thus lead to either enhancement or inhibition of inflammation, depending on other mediators present.

One puzzling aspect is that latexin contains no signal peptide or predicted hydrophobic segments that could mediate secretion. In this respect, latexin could resemble the serpin plasminogen activator inhibitor type 2 (PAI-2), which is a cytoplasmic protein located and regulated quite differently from its target, plasminogen activator (Costelloe et al., 1999). However, in mast cells, latexin has a granular localization and associates with a subpopulation of vesicles (Uratani et al., 2000), and we have confirmed that latexin is also expressed in a discrete granule population in macrophages (A. Burrows, D.A.H., and S.K., unpublished data).

Latexin is thought to be a noncompetitive inhibitor of CPA (Normant et al., 1995). This mode of inhibition makes it difficult to predict putative interaction sites, because the binding site may not necessarily involve the enzyme active site. Analysis of the latexin structure reveals a number of features that could represent protein interaction sites, without the need to invoke conformational changes. The electrostatic surface of latexin reveals a basic patch formed by residues from the α helices of both subdomains (Lys18 and Lys159). The two subdomains are arranged so that there is a cleft in this part of the structure that could accommodate a peptide chain. Another intriguing feature is the protruding nature of the loop incorporating a *cis*-peptide and comprising residues 121–131. Clearly, it is there for a purpose, since the *cis*-proline region is highly conserved throughout the wider latexin/TIG1 family. This conservation is indicative of a conserved structure and possibly a conserved function. Conversely, there is only one region in the protein sequences (Figure 1) that is hypervariable—the loop between β3 and β4. This loop varies in length (6–14 residues) and sequence (Figure 1) over all eight proteins, yet it is highly conserved within latexin or TIG1 subfamilies. The loop therefore represents a point of unusual variability in a seemingly well-conserved protein scaffold and will be of considerable interest should TIG1 proteins subsequently be shown not to have CPI activity.

The disparate sizes and sequences of latexin and the plant/parasite CPIs indicated a piori that they would encode very different protein folds, and this is borne out by the structural comparison (Figure 4). What was entirely unexpected was the striking similarity between the subdomains of latexin and proteins of the cystatin/monellin superfamily (Figure 4). This similarity suggests the possiblity that latexin may have cysteine protease inhibitor activity. However, the residues in cystatins that are involved in binding are conserved within the cystatin family, but are not present in latexin. Indeed, the sequence similarity between latexin and the cystatins is very low.

The sequence similarity between latexin and TIG1 suggests that the latter may have protease inhibitor activity, though this is not yet tested to our knowledge. Similarly, there is no evidence that latexin plays a tumor suppressor role, though its partner protein CPA3 has been shown to be induced in prostate cancer cells (Huang et al., 1999). However, if sequence identity between latexin and the C-terminal domain of TIG1 translates to structural and functional similarity, it is possible that TIG1 tumor suppressor function could be a consequence of extracellular proteolysis inhibition. This has parallels elsewhere in tumor biology; for example, the serine protease inhibitor maspin is a tumor suppressor

because it inhibits cell motility, invasion, and angiogenesis (Sager et al., 1997).

In summary, we have shown that proteolysis in general, and latexin in particular, play a role in the immune response, since the latexin gene is highly expressed in macrophages and its expression is further regulated by several proinflammatory stimuli. We solved the crystal structure of latexin, and this unexpectedly revealed a relationship between the carboxypeptidase inhibitor latexin and the cysteine protease inhibitors, cystatins. We identified a *cis*-proline loop in latexin that is likely to be important for function and that is conserved in the tumor suppressor protein TIG1.

Experimental Procedures

Differentiation of Bone Marrow-Derived Macrophages

Bone marrow-derived macrophages were obtained from femurs of a pool of 6- to 8-week-old male mice. Macrophages were differentiated from bone marrow progenitors in RPMI1640 (BRL), 10% fetal calf serum, and 10^4 U/ml (100 ng/ml) recombinant CSF-1 (a gift from Chiron, Emeryville, CA) for 6 days. Macrophages were seeded at 1×10^7 cells/ml and incubated with 10 ng/ml LPS from *Salmonella minnesota* (Sigma-Aldrich, St. Louis, MO). 3 × 10 cm dishes were harvested at each time point—unstimulated (time 0), 30 min, 2 hr, 7 hr, and 21 hr. RNA was extracted by using the RNeasy midi kit (Qiagen) according to manufacturer's instructions. Replica data were derived from independent RNA extractions of a different pool of 6- to 8-week-old mouse femurs.

Quantitative Real-Time PCR

Total RNA (2.5 μg) of each sample was treated with DNase 1 (Ambion, Austin, TX) and reverse-transcribed by using 17mer oligo-dT and the Superscript III RnaseH$^-$ reverse transcriptase kit, or the Superscript III First-Strand Synthesis system for RT-PCR (Invitrogen). Negative control samples (no first strand synthesis) were prepared by performing reactions in the absence of reverse transcriptase. The reaction after reverse transcription (20 μl) was diluted to 100 μl with water. Five μl diluted cDNA was used for quantitative real-time PCR performed by using the LightCycler-DNA Master SYBR Green I kit (Roche). The PCR was performed by using an ABI Prism machine (Applied Biosystems): 1 min hot start at 94°C, followed by 45 cycles of 1 s at 94°C, 10 s at 60°C, and 15 s at 72°C. cDNA levels during the linear phase of amplification were normalized against hypoxanthine phosphoribosyltransferase controls. Assays were done in triplicate, and mean ± SD was determined. Primers used for the amplification of murine latexin: forward 5′-TTCGAAGGAGAAATCGGCAA-3′ and reverse 5′-GGGATGTCC TGTGCTTCCAG-3′.

Expression and Purification

A pool of cDNA species generated by using mRNA extracted from murine bone marrow-derived macrophages treated with LPS over a time course of up to 24 hr (Wells et al., 2003a) was used as the template for PCR amplification. Mouse latexin cDNA (669 nucleotides) was amplified by using the forward primer 5′-CACC**ATG** GAAATCCCACCCACCCAC-3′ and reverse primer 5′-TCACTCCG CCTGCCCTTCC-3′ (start codon for translation is shown in bold) by using Eppendorf Triple Master blunt-ended proof-reading polymerase. The 50 μl PCR reaction contained 10 μl enzyme buffer, 100 ng of each primer, 1 μl 20 mM dNTPs, 0.5 μl cDNA, and 0.3 μl enzyme. The cycling conditions included initial denaturation for 2 min at 95°C, followed by 30 cycles of denaturation at 95°C for 30 s, annealing at 55°C for 45 s, and elongation at 68°C for 1 min. The PCR product was cloned into pENTR/D-TOPO vector with GATEWAY (Invitrogen). The latexin gene was transferred into pDEST-17 expression vector and expressed in *E. coli* as an N-terminal His-tag fusion protein.

The protein was expressed in *E. coli* by autoinduction (W. Studier, personal communication). A colony from an LB-Amp plate was inoculated into 1–2 ml defined minimal medium containing glucose as an energy source, thereby preventing expression of genes controlled by the lac-operon. After incubation at 37°C for a day, the culture was inoculated (1/100) into a rich medium containing glucose and lactose and then incubated overnight at 37°C. Typically, OD600 was 5–6 at harvest, and the yield of latexin was 100 mg/l culture. The His-tagged protein was purified by metal affinity chromatography (Talon, Clontech). After elution, the buffer was exchanged with 10 mM Hepes (pH 7.5), 150 mM NaCl, 10% glycerol, 1 mM DTT, and the protein was concentrated to ~50 mg/ml.

Selenomethionine (SeMet)-labeled latexin was produced as described previously for other proteins (Edeling et al., 2002) and purified in the same way as native protein. Incorporation of SeMet was verified by mass spectrometry by using a PE SCIEX API III triple-quadrupole mass spectrometer.

Crystal Structure

Crystals were obtained by hanging-drop vapor diffusion after 5–7 days by mixing 1 μl protein solution with 1 μl reservoir containing 1.8 M ammonium sulfate, 0.1 M cacodylate (pH 6.5) (space group $P4_32_12$ and unit cell dimensions a = b = 104.14 Å, c = 60.04 Å). Crystals of SeMet latexin were grown in the same way and appeared after 3–4 days. Crystals were flash-cooled after soaking for 10 s in a cryoprotectant containing 25% glycerol, 2.0 M ammonium sulfate, and 0.1 M cacodylate (pH 6.5). X-ray diffraction data (MAD and native) were measured at beamline 8.2.2 of the Advanced Light Source (ALS) at Lawrence Berkeley National Laboratory (LBNL, Berkeley, CA) and were processed and scaled by using HKL2000 (Otwinowski and Minor, 1997).

SOLVE (Terwilliger, 2003) was used to locate six seleniums and to provide initial phases for refinement (mean figure of merit = 0.7). Automatic model building was performed with ARP/WARP (Morris et al., 2003) within the CCP4 package (CCP4, 1994). The resulting model consisting of 179 amino acids was used as a starting point for model building in O (Jones et al., 1991) and refinement by maximum likelihood and individual B factor refinement against native data at 1.83 Å resolution with CNS (Brunger et al., 1998).

The final model includes residues 1–217 of latexin and 3 residues from the 28-residue tag (denoted –2, –1, and 0). The five C-terminal residues (218–222) were not included due to poor electron density.

Modeling and Analysis

Alignments between the proteins were generated by CLUSTALX (Jeanmougin et al., 1998) with default parameters. Models for the C-terminal region of rat, mouse, and human TIG1 corresponding to the latexin sequence were constructed by using MODELLER (Sali and Blundell, 1993) with mouse latexin structure as the template. The highest refinement level in HOMOLOGY (INSIGHTII, Accelrys) was used. The modeling procedure was iterative; in each iteration, 10 models were constructed and compared. The lowest energy structure was used for further refinement. The stereochemical quality of models was checked by using PROCHECK (Laskowski et al., 1993), as implemented in the Biotech validation suite at 1.9 Å resolution.

Sulfate binding pockets were identified by using GRID (Goodford, 1985) with a charged oxygen of a sulfate or phosphate used as a probe with grid spacing of 0.5 Å. Docking calculations were performed by using GOLD (v2.0) (Verdonk et al., 2003) for the binding of a pentasaccharide (1AZX [Jin et al., 1997]; energy minimized in BUILDER [INSIGHTII] by using the esff force-field) representing mast cell granule heparin. Fifty dockings were performed in the binding site defined as a 20 Å sphere centered on Arg171, and these were ranked according to the GoldScore fitness function (Verdonk et al., 2003). Cavity detection was not used; other parameters were set to defaults.

Acknowledgments

We thank staff at BL8.2.2 for help in data collection, Catherine Latham for help with data collection and processing, and Alun Jones for mass spectrometry. Crystallographic data were measured at the Advanced Light Source, which is supported by the Director, Office of Science, Office of Basic Energy Sciences, Materials Sciences

Division, of the U.S. Department of Energy under Contract No. DE-AC03-76SF00098 at the Lawrence Berkeley National Laboratory. This work was supported by a Postdoctoral Fellowship from the Swedish Foundation for International Cooperation in Research and Higher Education (STINT) to A.A., a National Health and Medical Research Council of Australia Senior Research Fellowship to B.K., an Australian Research Council (ARC) Senior Research Fellowship to J.L.M., and by the Cooperative Research Centre for Chronic Inflammatory Disease, and an ARC grant to J.L.M. and B.K.

Received: October 28, 2004
Revised: December 7, 2004
Accepted: December 7, 2004
Published: February 8, 2005

References

Arimatsu, Y. (1994). Latexin: a molecular marker for regional specification in the neocortex. Neurosci. Res. *20*, 131–135.

Bai, W.Z., Ishida, M., and Arimatsu, Y. (2004). Chemically defined feedback connections from infragranular layers of sensory association cortices in the rat. Neuroscience *123*, 257–267.

Balint, E., Lapointe, D., Drissi, H., Van Der Meijden, C., Young, D.W., Van Wijnen, A.J., Stein, J.L., Stein, G.S., and Lian, J.B. (2003). Phenotype discovery by gene expression profiling: mapping of biological processes linked to BMP-2-mediated osteoblast differentiation. J. Cell. Biochem. *89*, 401–426.

Bode, W., Engh, R., Musil, D., Thiele, U., Huber, R., Karshikov, A., Brzin, J., Kos, J., and Turk, V. (1988). The 2.0 Å X-ray crystal structure of chicken egg white cystatin and its possible mode of interaction with cysteine proteinases. EMBO J. *7*, 2593–2599.

Brunger, A.T., Adams, P.D., Clore, G.M., DeLano, W.L., Gros, P., Grosse-Kunstleve, R.W., Jiang, J.S., Kuszewski, J., Nilges, M., Pannu, N.S., et al. (1998). Crystallography & NMR system: a new software suite for macromolecular structure determination. Acta Crystallogr. D Biol. Crystallogr. *54*, 905–921.

CCP4 (Collaborative Computational Project, Number 4)(1994). The CCP4 suite: programs for protein crystallography. Acta Crystallogr. D Biol. Crystallogr. *50*, 760–763.

Costelloe, E.O., Stacey, K.J., Antalis, T.M., and Hume, D.A. (1999). Regulation of the plasminogen activator inhibitor-2 (PAI-2) gene in murine macrophages. Demonstration of a novel pattern of responsiveness to bacterial endotoxin. J. Leukoc. Biol. *66*, 172–182.

Edeling, M.A., Guddat, L.W., Fabianek, R.A., Thony-Meyer, L., and Martin, J.L. (2002). Structure of CcmG/DsbE at 1.14 Å resolution: high-fidelity reducing activity in an indiscriminately oxidizing environment. Structure (Camb.) *10*, 973–979.

Esnouf, R.M. (1999). Further additions to MolScript version 1.4, including reading and contouring of electron-density maps. Acta Crystallogr. D Biol. Crystallogr. *55*, 938–940.

Ginalski, K., Elofsson, A., Fischer, D., and Rychlewski, L. (2003). 3D-Jury: a simple approach to improve protein structure predictions. Bioinformatics *19*, 1015–1018.

Goodford, P.J. (1985). A computational procedure for determining energetically favorable binding sites on biologically important macromolecules. J. Med. Chem. *28*, 849–857.

Hadkar, V., and Skidgel, R.A. (2001). Carboxypeptidase D is upregulated in raw 264.7 macrophages and stimulates nitric oxide synthesis by cells in arginine-free medium. Mol. Pharmacol. *59*, 1324–1332.

Hincke, M.T., Gautron, J., Mann, K., Panheleux, M., McKee, M.D., Bain, M., Solomon, S.E., and Nys, Y. (2003). Purification of ovocalyxin-32, a novel chicken eggshell matrix protein. Connect. Tissue Res. *44* (*Suppl 1*), 16–19.

Holm, L., and Sander, C. (1993). Protein structure comparison by alignment of distance matrices. J. Mol. Biol. *233*, 123–138.

Huang, H., Reed, C.P., Zhang, J.S., Shridhar, V., Wang, L., and Smith, D.I. (1999). Carboxypeptidase A3 (CPA3): a novel gene highly induced by histone deacetylase inhibitors during differentiation of prostate epithelial cancer cells. Cancer Res. *59*, 2981–2988.

Jaffray, C., Mendez, C., Denham, W., Carter, G., and Norman, J. (2000). Specific pancreatic enzymes activate macrophages to produce tumor necrosis factor-alpha: role of nuclear factor kappa B and inhibitory kappa B proteins. J. Gastrointest. Surg. *4*, 370–377.

Jeanmougin, F., Thompson, J.D., Gouy, M., Higgins, D.G., and Gibson, T.J. (1998). Multiple sequence alignment with Clustal X. Trends Biochem. Sci. *23*, 403–405.

Ji, B., Chen, X.Q., Misek, D.E., Kuick, R., Hanash, S., Ernst, S., Najarian, R., and Logsdon, C.D. (2003). Pancreatic gene expression during the initiation of acute pancreatitis: identification of EGR-1 as a key regulator. Physiol. Genomics *14*, 59–72.

Jin, L., Abrahams, J.P., Skinner, R., Petitou, M., Pike, R.N., and Carrell, R.W. (1997). The anticoagulant activation of antithrombin by heparin. Proc. Natl. Acad. Sci. USA *94*, 14683–14688.

Jing, C., El-Ghany, M.A., Beesley, C., Foster, C.S., Rudland, P.S., Smith, P., and Ke, Y. (2002). Tazarotene-induced gene 1 (TIG1) expression in prostate carcinomas and its relationship to tumorigenicity. J. Natl. Cancer Inst. *94*, 482–490.

Jones, T.A., Zou, J.Y., and Cowan, S.W. (1991). Improved methods for building protein models in electron density maps and the location of errors in these models. Acta Crystallogr. A *47*, 110–119.

Kraulis, P.J. (1991). MOLSCRIPT: a program to produce both detailed and schematic plots of protein structures. J. Appl. Crystallogr. *24*, 946–950.

Laskowski, R.A., MacArthur, M.W., Moss, D.S., and Thornton, J.M. (1993). PROCHECK: a program to check the stereochemical quality of protein structures. J. Appl. Crystallogr. *26*, 283–291.

Merritt, E.A., and Murphy, M.E.P. (1994). Raster3D Version 2.0. A program for photorealistic molecular graphics. Acta Crystallogr. D Biol. Crystallogr. *50*, 869–873.

Metsarinne, K.P., Vehmaan-Kreula, P., Kovanen, P.T., Saijonmaa, O., Baumann, M., Wang, Y., Nyman, T., Fyhrquist, F.Y., and Eklund, K.K. (2002). Activated mast cells increase the level of endothelin-1 mRNA in cocultured endothelial cells and degrade the secreted peptide. Arterioscler. Thromb. Vasc. Biol. *22*, 268–273.

Morris, R.J., Perrakis, A., and Lamzin, V.S. (2003). ARP/wARP and automatic interpretation of protein electron density maps. Methods Enzymol. *374*, 229–244.

Murzin, A.G., Brenner, S.E., Hubbard, T., and Chothia, C. (1995). SCOP: a structural classification of proteins database for the investigation of sequences and structures. J. Mol. Biol. *247*, 536–540.

Nagpal, S., Patel, S., Asano, A., Johnson, A., Duvic, M., and Chandraratna, R. (1996). Tazarotene-induced gene 1 (TIG1), a novel retinoic acid receptor-responsive gene in skin. J. Invest. Dermatol. *106*, 269–274.

Neuvirth, H., Raz, R., and Schreiber, G. (2004). ProMate: a structure based prediction program to identify the location of protein-protein binding sites. J. Mol. Biol. *338*, 181–199.

Nicholls, A., Bharadwaj, R., and Honig, B. (1993). GRASP: graphical representation and analysis of surface properties. Biophys. J. *64*, A116.

Normant, E., Martres, M.P., Schwartz, J.C., and Gros, C. (1995). Purification, cDNA cloning, functional expression, and characterization of a 26-kDa endogenous mammalian carboxypeptidase inhibitor. Proc. Natl. Acad. Sci. USA *92*, 12225–12229.

Otwinowski, Z., and Minor, W. (1997). Processing of X-ray diffraction data collected in oscillation mode. Methods Enzymol. *276*, 307–326.

Reddanna, P., Sandeep Prabhu, K., Whelan, J., and Channa Reddy, C. (2003). Carboxypeptidase A-catalyzed direct conversion of leukotriene C4 to leukotriene F4. Arch. Biochem. Biophys. *413*, 158–163.

Rees, D.C., and Lipscomb, W.N. (1982). Refined crystal structure of the potato inhibitor complex of carboxypeptidase A at 2.5 Å resolution. J. Mol. Biol. *160*, 475–498.

Rehli, M., Krause, S.W., and Andreesen, R. (2000). The membrane-bound ectopeptidase CPM as a marker of macrophage maturation in vitro and in vivo. Adv. Exp. Med. Biol. *477*, 205–216.

Reverter, D., Fernandez-Catalan, C., Baumgartner, R., Pfander, R.,

Huber, R., Bode, W., Vendrell, J., Holak, T.A., and Aviles, F.X. (2000). Structure of a novel leech carboxypeptidase inhibitor determined free in solution and in complex with human carboxypeptidase A2. Nat. Struct. Biol. *7*, 322–328.

Sager, R., Sheng, S., Pemberton, P., and Hendrix, M.J. (1997). Maspin. A tumor suppressing serpin. Adv. Exp. Med. Biol. *425*, 77–88.

Sali, A., and Blundell, T.L. (1993). Comparative protein modelling by satisfaction of spatial restraints. J. Mol. Biol. *234*, 779–815.

Somoza, J.R., Jiang, F., Tong, L., Kang, C.H., Cho, J.M., and Kim, S.H. (1993). Two crystal structures of a potently sweet protein. Natural monellin at 2.75 Å resolution and single-chain monellin at 1.7 Å resolution. J. Mol. Biol. *234*, 390–404.

Stubbs, M.T., Laber, B., Bode, W., Huber, R., Jerala, R., Lenarcic, B., and Turk, V. (1990). The refined 2.4 Å X-ray crystal structure of recombinant human stefin B in complex with the cysteine proteinase papain: a novel type of proteinase inhibitor interaction. EMBO J. *9*, 1939–1947.

Terwilliger, T.C. (2003). SOLVE and RESOLVE: automated structure solution and density modification. Methods Enzymol. *374*, 22–37.

Uratani, Y., Takiguchi-Hayashi, K., Miyasaka, N., Sato, M., Jin, M., and Arimatsu, Y. (2000). Latexin, a carboxypeptidase A inhibitor, is expressed in rat peritoneal mast cells and is associated with granular structures distinct from secretory granules and lysosomes. Biochem. J. *346*, 817–826.

Verdonk, M.L., Cole, J.C., Hartshorn, M.J., Murray, C.W., and Taylor, R.D. (2003). Improved protein-ligand docking using GOLD. Proteins *52*, 609–623.

Wells, C.A., Ravasi, T., Faulkner, G.J., Carninci, P., Okazaki, Y., Hayashizaki, Y., Sweet, M., Wainwright, B.J., and Hume, D.A. (2003a). Genetic control of the innate immune response. BMC Immunol. *4*, 5.

Wells, C.A., Ravasi, T., Sultana, R., Yagi, K., Carninci, P., Bono, H., Faulkner, G., Okazaki, Y., Quackenbush, J., Hume, D.A., and Lyons, P.A. (2003b). Continued discovery of transcriptional units expressed in cells of the mouse mononuclear phagocyte lineage. Genome Res. *13*, 1360–1365.

Accession Numbers

Coordinates are deposited with the PDB under accession code 1WNH.